



## Insufficient mass spectrometric detection of synthesized peroxy acids from $\alpha$ -pinene ozonolysis

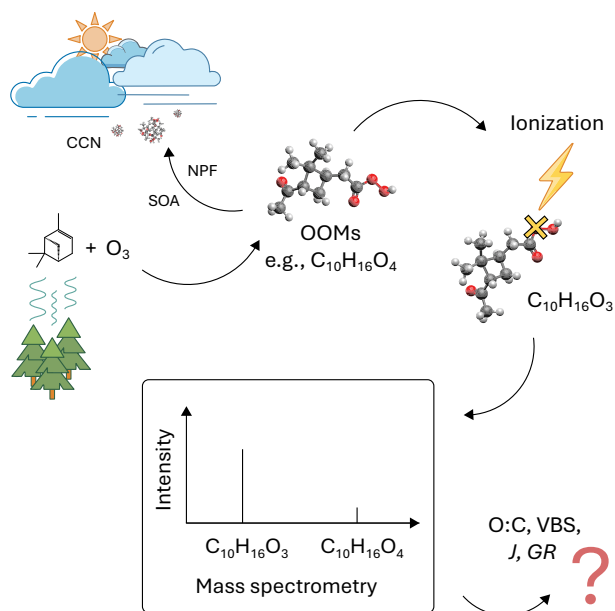
Markus Tischberger<sup>1</sup>, Rulan Verma<sup>1</sup>, Johanna Breinsperger<sup>2</sup>, David Schachamayr<sup>2</sup>, Marco Lair<sup>1</sup>, Melanie Opacak<sup>1</sup>, Peter Gärtner<sup>2</sup>, Hinrich Grothe<sup>1</sup>, Maximilian Kaiser<sup>2</sup>, and Dominik Stolzenburg<sup>1</sup>

<sup>1</sup>Institute of Materials Chemistry, TU Wien, Getreidemarkt 9, 1060 Vienna, Austria

<sup>2</sup>Institute of Applied Synthetic Chemistry, TU Wien, Getreidemarkt 9, 1060 Vienna, Austria

**Correspondence:** Maximilian Kaiser (maximilian.kaiser@tuwien.ac.at) and Dominik Stolzenburg (dominik.stolzenburg@tuwien.ac.at)

**Abstract.** Biogenic volatile organic compounds (BVOCs) are major precursors of secondary organic aerosol (SOA) and new particle formation (NPF), and therefore play an important role in the climate system, altering the abundance of cloud condensation nuclei (CCN). Ozonolysis of the most atmospherically abundant monoterpene,  $\alpha$ -pinene, generates RO<sub>2</sub> radicals which undergo autoxidation, resulting in the formation of oxygenated organic molecules (OOMs) with low volatility, an essential step in nucleation and early particle growth. However, quantitative interpretation of widely used mass spectrometric OOM measurements remains limited by reagent-ion selectivity and the lack of authentic monomeric standards, an issue that is particularly important for hydroperoxides and peroxy acids, which constitute a significant fraction of autoxidation products. Here, we synthesize two  $\alpha$ -pinene-derived monomeric OOM standards, peroxy norpinonic acid (PNPA; C<sub>9</sub>H<sub>14</sub>O<sub>4</sub>) and peroxy pinonic acid (PPA; C<sub>10</sub>H<sub>16</sub>O<sub>4</sub>), and confirm their structures by <sup>1</sup>H and <sup>13</sup>C NMR. We then evaluate their detectability using a MION-Orbitrap operated with nitrate (NO<sub>3</sub><sup>-</sup>) and uronium (CH<sub>5</sub>N<sub>2</sub>O<sup>+</sup>) chemical ionization and compare these gas-phase schemes to heated electrospray ionization (H-ESI). NMR shows that freshly prepared standards are dominated by peroxy acids and contain only a fraction of the corresponding carboxylic acids, whereas Orbitrap measurements consistently yield substantially lower peroxy-to-carboxylic-acid ratios. These ratios vary strongly across ionization modes, with greater apparent peroxy acid loss under harder (de)protonation and improved, though still incomplete, preservation under softer nitrate and uronium adduct formation, indicating that the decomposition originates during ionization. Notably, uronium provides significantly higher sensitivity for these moderately oxygenated compounds, complementing nitrate's strong selectivity toward highly oxygenated molecules (HOMs). Together, our results suggest that peroxy acids formed via  $\alpha$ -pinene autoxidation may be systematically under-quantified by commonly used mass spectrometric approaches, with implications for O:C assignments, volatility-basis-set derivations, and inferred atmospheric process rates of nucleation and early particle growth.



20

## 1 Introduction

Biogenic volatile organic compounds (BVOCs) are key precursors of secondary organic aerosol (SOA) (Hodzic et al., 2016), a major component of atmospheric particulate matter (Zhang et al., 2007; Hallquist et al., 2009; Jimenez et al., 2009) with profound implications for climate (IPCC, 2021) and human health (HEI, 2025; IHME, 2025). New particle formation (NPF), where molecules form thermodynamically stable clusters through nucleation and continue to grow to larger sizes (Kulmala, 2003), is the dominant source in terms of aerosol particle number concentration across most of the troposphere (Yu and Luo, 2009; Gordon et al., 2017) and contributes significantly to the particle and cloud condensation nuclei (CCN) budget in the continental boundary layer (Reddington et al., 2011; Fountoukis et al., 2012; Matsui et al., 2013; Lupascu et al., 2015; Posner and Pandis, 2015; Cai et al., 2016). Monoterpenes and particularly  $\alpha$ -pinene ( $C_{10}H_{16}$ ) emitted by trees contribute significantly to global BVOC emissions (Sindelarova et al., 2022) and have therefore become central to studies of SOA and NPF.

Upon reaction with atmospheric ozone,  $\alpha$ -pinene ozonolysis is initiated, leading to the formation of peroxy radicals ( $RO_2$ ) (Ehn et al., 2014; Kurtén et al., 2015) which can undergo autoxidation. In this process, consecutive intramolecular H-shifts followed by rapid  $O_2$  additions produce increasingly oxygenated organic molecules (OOMs), often containing hydroperoxide [ $-OOH$ ] or peroxy acid [ $-(C=O)OOH$ ] functionalities. Their volatility can decrease to the regime of (extremely) low volatility organic compounds ((E)LVOC), enabling condensation onto existing molecular clusters or sufficiently large particles, or even direct participation in nucleation driven solely by ELVOC interactions in the case of highly oxygenated organic molecules (HOMs) (Ehn et al., 2014; Kirkby et al., 2016; Tröstl et al., 2016; Bianchi et al., 2019).

OOMs govern key stages of continental boundary layer NPF: covalently bound dimers serve as the main nucleators driving



cluster formation (Kirkby et al., 2016; Elm et al., 2017; Bianchi et al., 2019), while OOM monomers drive early particle growth  
40 due to their higher concentrations and low saturation vapor pressures (Tröstl et al., 2016; Qi et al., 2018; Stolzenburg et al.,  
2018).

The primary technique for measuring OOMs is chemical ionization (CI) mass spectrometry using nitrate ( $\text{NO}_3^-$ ) as reagent  
ion, with the CI-API-TOF being an especially prominent instrument (Bianchi et al., 2019). However, nitrate chemical ion-  
ization mass spectrometers (CIMS) are less sensitive towards less oxygenated analytes (Riva et al., 2019b), which are still  
45 decisive for particle growth, especially at lower temperatures (Stolzenburg et al., 2018). Orbitrap mass spectrometry coupled  
with the multischeme chemical ionization inlet (MION) is an emerging and promising technique (Rissanen et al., 2019; Riva  
et al., 2019a; Cai et al., 2024). The ultra-high resolution ( $> 100,000$ ), fast polarity and reagent switching, and multi-pressure  
scheme of the MION-Orbitrap enable the measurement of the full distribution of precursor molecules and their progressively  
oxygenated reaction products in atmospheric environments (Rissanen et al., 2019; Cai et al., 2024; Shcherbinin et al., 2024).

50 Two key challenges remain. First, any ionization reagent is inherently selective, making complete capture of all molecu-  
lar species unattainable. Continued development of reagents with broader coverage is therefore essential. Second, authentic  
monomeric OOM standards, particularly those featuring peroxy acid functionalities, are not commercially available. The ab-  
sence of suitable OOM standards critically constrains both the study of their detection by CIMS and the development of robust  
and precise calibration methods (Alage et al., 2024). Because their ionization efficiencies remain unknown, quantitative inter-  
55 pretation of OOM concentrations in the atmosphere, and thus accurate model representation, remains severely limited. While  
the synthesis of OOM dimers has been demonstrated (Kenseth et al., 2020, 2023; Li et al., 2024), only a few studies have  
attempted OOM monomer synthesis, successfully producing  $\alpha$ -pinene-derived monoperoxy-pinonic acid (Steimer et al., 2018)  
and hydroxy hydroperoxides (Mettke et al., 2022).

In this study, we synthesized two OOM monomers derived from  $\alpha$ -pinene ozonolysis with molecular formulas  $\text{C}_9\text{H}_{14}\text{O}_4$  and  
60  $\text{C}_{10}\text{H}_{16}\text{O}_4$ , referred to as peroxy norpinonic acid (PNPA) and peroxy pinonic acid (PPA), respectively (structures depicted in  
Fig. 1). They represent the corresponding peroxy acids of norpinonic acid (NPA;  $\text{C}_9\text{H}_{14}\text{O}_3$ ) and pinonic acid (PA;  $\text{C}_{10}\text{H}_{16}\text{O}_3$ ),  
which are major oxidation products of  $\alpha$ -pinene (Wilson et al., 1972; Hatakeyama et al., 1989; Kavouras et al., 1999; Yu et al.,  
1999). Both standards contain four oxygen atoms, classifying them as moderately oxygenated molecules (MOMs). Notably,  
the presence of peroxy acid functional groups may render our synthesized MOM standards valuable proxies also for HOMs.  
65 We confirmed their structures via  $^1\text{H}$  and  $^{13}\text{C}$  NMR (nuclear magnetic resonance) spectroscopy and subsequently investigated  
their detection with a MION-Orbitrap operated with nitrate ( $\text{NO}_3^-$ ) and uronium ( $\text{CH}_5\text{N}_2\text{O}^+$ ) (Shcherbinin et al., 2025). The  
gas-phase ionization was also compared to heated electrospray ionization (H-ESI). We show that peroxy acids exhibit strong  
variability in their instrument response across different ionization schemes, indicating that their abundance may be substantially  
underestimated in atmospheric studies.

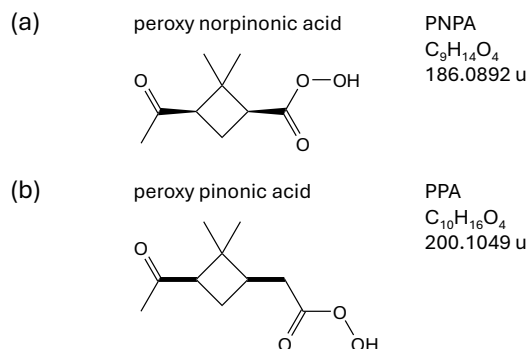


**Figure 1.** Synthesized oxygenated organic molecule (OOM) monomers: (a) peroxy norpinonic acid (PNPA;  $C_9H_{14}O_4$ ; exact mass 186.0892 u) and (b) peroxy pinonic acid (PPA;  $C_{10}H_{16}O_4$ ; exact mass 200.1049 u).

## 70 2 Materials and methods

### 2.1 Synthesized OOM standards

Figure 1 presents the molecular structures of our synthesized OOM monomers along with their full names, abbreviations, chemical formulas, and exact masses. Peroxy norpinonic acid (PNPA;  $C_9H_{14}O_4$ ) and peroxy pinonic acid (PPA;  $C_{10}H_{16}O_4$ ) exhibit exact masses of 186.0892 u and 200.1049 u, respectively. They were synthesized according to the procedure outlined  
75 in Appendix A, measured with  $^1H$  and  $^{13}C$  NMR (Bruker AC 400 MHz NMR spectrometer), and immediately prepared for and transferred to the mass spectrometric experimental setup.

### 2.2 Laboratory experiment

Figure 2 schematically illustrates the experimental setup comprising two pathways. In pathway (a), the synthesized standards were dissolved in deuterated chloroform (sample concentration:  $\sim 75 \text{ mg mL}^{-1}$ ) and introduced into an evaporator (solution  
80 volume: 0.6 mL), which was temperature-regulated to  $20^\circ\text{C}$  by water circulating through its double wall from a thermal bath (Thermo Fisher Scientific Inc., Fisherbrand Isotemp 4100 R20F). A continuous stream of  $2 \text{ L min}^{-1}$  clean and dry compressed air was directed over the sample. The resulting vapor was diluted with  $18 \text{ L min}^{-1}$  of air in a sheath-flow configuration and transferred into the MION2 (Karsa Oy), where alternating gas-phase chemical ionization with nitrate ( $\text{NO}_3^-$ ) and uronium ( $\text{CH}_5\text{N}_2\text{O}^+$ ) reagent ions at atmospheric pressure was performed. Analyte ions were subsequently measured using an Orbitrap  
85 Exploris MX mass spectrometer (Thermo Fisher Scientific Inc.) with a mass resolution of 180,000 (at  $m/z$  200). The sample lines were kept as short as possible, with the PTFE tube connecting the evaporator to the stainless steel inlet measuring 70 mm. In pathway (b), the synthesized standards were dissolved in acetonitrile (sample concentration:  $5 \times 10^{-3} \text{ mg mL}^{-1}$ ), filtered, and drawn into a syringe (solution volume: 0.4 mL). The sample solution was delivered at a flow rate of  $20 \mu\text{L min}^{-1}$  through

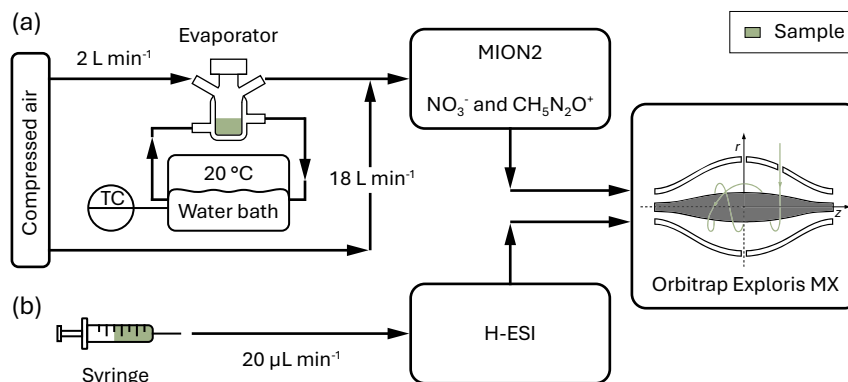


**Figure 2.** Laboratory experimental setup illustrating two independent approaches: (a) sample evaporation and gas-phase chemical ionization at atmospheric pressure using the multischeme chemical ionization inlet (MION2), and (b) liquid sample introduction and heated electro-spray ionization (H-ESI). Orbitrap mass analyzer schematic adapted with permission from Thermo Fisher Scientific Inc. Abbreviations: TC: temperature controller;  $\text{NO}_3^-$ : nitrate;  $\text{CH}_5\text{N}_2\text{O}^+$ : uronium.

the capillaries into the H-ESI source, where ionization occurred prior to introduction into the Orbitrap.

90 The Orbitrap mass spectrometer was operated in negative polarity for nitrate and H-ESI measurements, and in positive polarity for uronium measurements, with a full scan range of 50–750  $m/z$ , the RF Lens set to 70 %, standard AGC Target settings, and a maximum injection time of 100 ms. For MION2, the ion transfer tube temperature was set to 100 °C, whereas for H-ESI it was set to 320 °C. For H-ESI, the vaporizer temperature was 75 °C and the ion spray voltage was 2300 V. Mass calibration was performed using the Pierce FlexMix Calibration Solution (Thermo Fisher Scientific Inc.). Inter- and intra-sample variability

95 were evaluated by repeating the synthesis and experimental procedures multiple times. PNPA was synthesized three times, yielding a total of six experimental repetitions. PPA was synthesized once and analyzed across three experimental repetitions. The experiments were also repeated with pure pinonic acid (PA) and commercial *meta*-Chloroperoxybenzoic acid (*m*CPBA ( $\text{C}_7\text{H}_5\text{ClO}_3$ );  $\leq 77\%$  assay; remainder predominantly *meta*-Chlorobenzoic acid (*m*CBA) ( $\text{C}_7\text{H}_5\text{ClO}_2$ ) and water), each conducted three times.

### 100 2.3 Data analysis

Mass spectra were acquired using Tune (Thermo Fisher Scientific Inc.). Four-minute averaged spectra were exported via FreeStyle (Thermo Fisher Scientific Inc.), and mass peaks of interest were extracted and normalized to primary ions for nitrate and uronium, and to the total ion count (TIC) for H-ESI. In MION2, ionization occurred predominantly through (de)protonation and adduct formation, whereas H-ESI primarily achieved analyte ionization via deprotonation. Table 1 summarizes the masses

105 of interest for each ionization method and OOM standard, including those corresponding to the carboxylic acids norpinonic



**Table 1.** Ionization methods, associated ion species of interest, and exact masses for ions generated from the synthesized molecules (PNPA ( $C_9H_{14}O_4$ ), PPA ( $C_{10}H_{16}O_4$ )) and their corresponding carboxylic acids (NPA ( $C_9H_{14}O_3$ ), PA ( $C_{10}H_{16}O_3$ )).

Ionization method	Ion species	Molecules and exact ion masses (u)			
		$C_9H_{14}O_4$	$C_9H_{14}O_3$	$C_{10}H_{16}O_4$	$C_{10}H_{16}O_3$
MION2 (nitrate) & H-ESI	$[M - H]^-$	185.0814	169.0865	199.0970	183.1021
MION2 (uronium)	$[M + H]^+$	187.0970	171.1021	201.1127	185.1178
MION2 (nitrate)	$[M + NO_3]^-$	248.0770	232.0821	262.0927	246.0978
MION2 (uronium)	$[M + CH_5N_2O]^+$	247.1294	231.1345	261.1450	245.1501

acid (NPA;  $C_9H_{14}O_3$ ) and pinonic acid (PA;  $C_{10}H_{16}O_3$ ). The statistical significance of all sample peaks was verified by applying a  $3\sigma$  threshold derived from blank measurements.

### 3 Results and discussion

Due to the synthesis procedure, each sample of synthesized standards contained a specific ratio of peroxy acids to their corresponding carboxylic acids. Figure 3 displays these ratios for both OOM standards measured by NMR and Orbitrap immediately after synthesis, as described in the previous section. Orbitrap ratios were computed from normalized peak intensities and averaged across repeated experiments; the plotted values represent the mean and the standard uncertainty derived from all measurements. NMR yielded the highest ratios (4.4 for PNPA and 4.7 for PPA), indicating that the freshly prepared standards were dominated by peroxy acids. In contrast, Orbitrap measurements produced significantly lower ratios. The only cases approaching or exceeding unity were nitrate adduct ionization for PNPA ( $0.87 \pm 0.22$ ; consistent with unity within uncertainty) and uronium adduct ionization for PPA (1.77), both indicating a higher abundance of peroxy acids than carboxylic acids, yet still yielding ratios substantially lower than those determined by NMR. Deprotonation and protonation yielded considerably lower ratios (0.03 to 0.39). These discrepancies reflect fundamental differences between techniques: NMR reports bulk composition in a fully non-perturbative, sample-preserving manner, whereas mass spectrometry reports only the fraction of molecules that successfully transfer, ionize, and survive to detection – processes that are inherently sensitive to evaporation and ionization efficiency, in-source chemistry, and matrix effects such as ion suppression. Consequently, the measured mass spectrometric signal response represents an interplay between (i) evaporation and transport kinetics from the liquid sample solution into the gas phase and onward to the Orbitrap, (ii) intrinsic molecular properties such as carbon number, functional group arrangement, and O–O bond lability, and (iii) the ionization pathway, including its efficiency, softness or hardness (adduct formation vs. (de)protonation), clustering energetics, and reagent selectivity.

This framework also clarifies the role of our gas-phase experimental approach (pathway (a) in Fig. 2), which relies on evaporation of the liquid sample in the evaporator followed by transport of the volatilized molecules in an airstream toward the

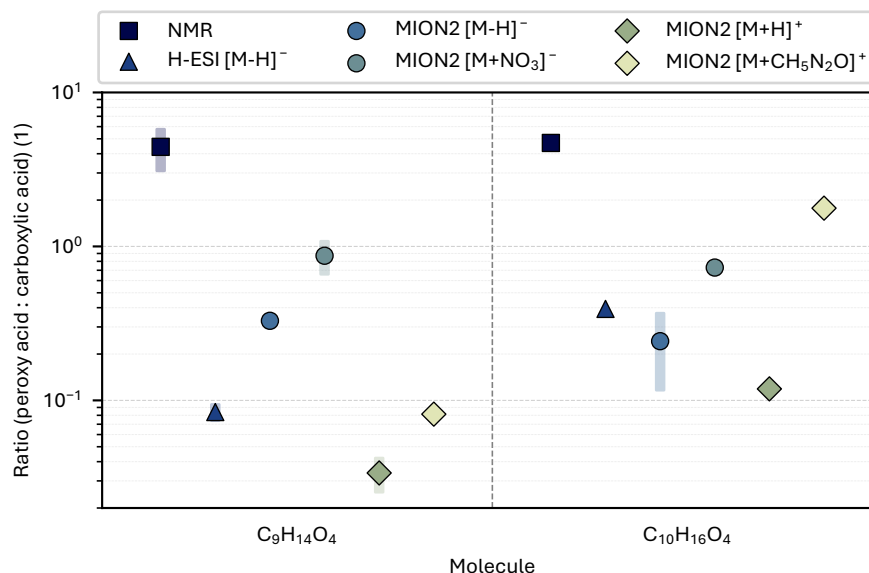


**Figure 3.** Ratios of peroxy acids to their corresponding carboxylic acids for PNPA (C<sub>9</sub>H<sub>14</sub>O<sub>4</sub>) and PPA (C<sub>10</sub>H<sub>16</sub>O<sub>4</sub>) measured by NMR and MION- and H-ESI-Orbitrap. Symbols represent mean ratios, and shaded areas indicate standard uncertainties calculated from all repeated syntheses and measurements. If no error bar is visible, it is obscured by the symbol. Circles represent MION-Orbitrap operated with nitrate, and diamonds represent MION-Orbitrap operated with uronium.

MION-Orbitrap. Under these conditions, any observed ratio between peroxy acids and carboxylic acids may be influenced by differences in their inherent volatilities. Table 2 lists the saturation mass concentrations and liquid vapor pressures of the synthesized OOM standards, *m*CPBA, and their corresponding carboxylic acids, calculated using the SIMPOL.1 group contribution method (Pankow and Asher, 2008). Their saturation mass concentrations, which are on the order of 10<sup>2</sup> to 10<sup>5</sup> μg m<sup>-3</sup>, classify these molecules as intermediate volatility organic compounds (IVOCs) (Donahue et al., 2009; Stolzenburg et al., 2022).

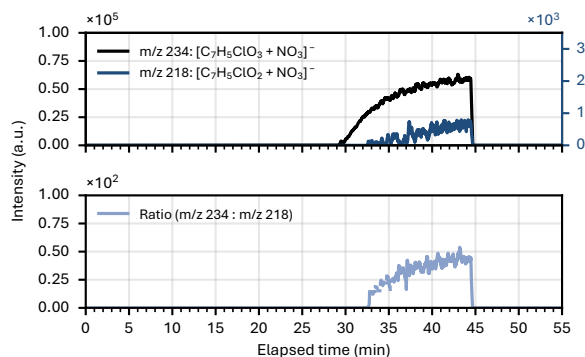
These calculations predict that, at 20 °C, peroxy acids exhibit higher liquid vapor pressures and saturation concentrations, and therefore greater volatility, than the corresponding carboxylic acids (Table 2). Under these conditions, we would therefore expect preferential evaporation and more efficient transfer of peroxy acids into the gas stream and to the MION2, resulting in an even higher ratio of peroxy to carboxylic acids reaching MION2, being ionized, and ultimately detected in the Orbitrap than measured by NMR.

Figure 4 shows a representative time trace of the nitrate adduct signals for *m*CPBA and *m*CBA, along with the temporal evolution of the peroxy-to-carboxylic-acid ratio. The initial ~25 min correspond to blank measurements, while the pronounced increase in signal intensity at ~30 min indicates the start of sample evaporation following introduction into the evaporator. Consistent with the SIMPOL.1 group contribution predictions at 20 °C, where the peroxy acid functional group yields a higher vapor pressure and therefore a higher saturation concentration than the corresponding carboxylic acid group, the *m*CPBA control experiment exhibits the expected volatility contrast: *m*CPBA produces a strong, early-rising nitrate adduct signal,



**Table 2.** Saturation mass concentrations  $\log_{10}(c^{\circ})$  and liquid vapor pressures  $p_L^{\circ}$  for the synthesized molecules (PNPA ( $C_9H_{14}O_4$ ), PPA ( $C_{10}H_{16}O_4$ )), *meta*-Chloroperoxybenzoic acid (*m*CPBA;  $C_7H_5ClO_3$ ), and their corresponding carboxylic acids (NPA ( $C_9H_{14}O_3$ ), PA ( $C_{10}H_{16}O_3$ ), and *meta*-Chlorobenzoic acid (*m*CBA;  $C_7H_5ClO_2$ )), calculated using the SIMPOL.1 group contribution method (Pankow and Asher, 2008).

Molecule	Saturation mass concentration $\log_{10}(c^{\circ}[\mu\text{g m}^{-3}])$	Vapor pressure $p_L^{\circ}$ (Pa)
$C_9H_{14}O_4$	4.32	$2.72 \times 10^{-1}$
$C_9H_{14}O_3$	3.18	$2.16 \times 10^{-2}$
$C_{10}H_{16}O_4$	3.91	$9.94 \times 10^{-2}$
$C_{10}H_{16}O_3$	2.78	$7.90 \times 10^{-3}$
$C_7H_5ClO_3$	5.43	$3.81 \times 10^0$
$C_7H_5ClO_2$	4.29	$3.03 \times 10^{-1}$



**Figure 4.** Extracted-ion chromatogram of the nitrate adduct ions of *meta*-Chloroperoxybenzoic acid (*m*CPBA;  $C_7H_5ClO_3$ ;  $m/z$  234 for the nitrate adduct) and *meta*-Chlorobenzoic acid (*m*CBA;  $C_7H_5ClO_2$ ;  $m/z$  218 for the nitrate adduct). Absolute intensities and the ratio (peroxy acid to carboxylic acid) are shown.

whereas the *m*CBA signal appears more slowly and at substantially lower intensity. This difference in evaporation kinetics is reflected in the peroxy-to-carboxylic-acid ratio, which increases gradually over  $\sim 12$  min before approaching a steady plateau, indicating the time required for the less volatile *m*CBA to accumulate in the gas phase. The peroxy acid signal is roughly two orders of magnitude higher than that of the carboxylic acid, consistent with both its greater volatility and its larger fraction in the technical *m*CPBA mixture. Together, these observations reflect the behavior predicted by SIMPOL.1 and demonstrate the characteristic signature of two species with distinctly different volatilities evaporating independently and being transferred to the MION2 and ultimately detected in the Orbitrap.

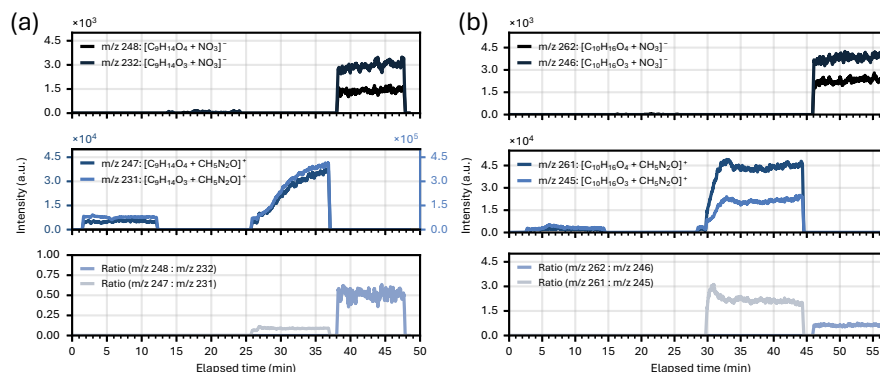


**Figure 5.** Extracted-ion chromatograms of the nitrate and uronium adduct ions of (a) peroxy norpinonic acid (PNPA;  $C_9H_{14}O_4$ ;  $m/z$  248 for the nitrate adduct and 247 for the uronium adduct) and norpinonic acid (NPA;  $C_9H_{14}O_3$ ;  $m/z$  232 for the nitrate adduct and 231 for the uronium adduct) and (b) peroxy pinonic acid (PPA;  $C_{10}H_{16}O_4$ ;  $m/z$  262 for the nitrate adduct and 261 for the uronium adduct) and pinonic acid (PA;  $C_{10}H_{16}O_3$ ;  $m/z$  246 for the nitrate adduct and 245 for the uronium adduct). Absolute intensities and the ratios (peroxy acid to carboxylic acid) are shown.

Figure 5 shows representative time traces for the nitrate and uronium adduct signals of PNPA/NPA and PPA/PA, respectively, together with the time evolution of the peroxy-to-carboxylic-acid ratio. The first  $\sim 25$  min capture blank measurements in both ionization modes. The onset of sample introduction into the evaporator and subsequent evaporation is evident from the sharp intensity increases in uronium mode at  $\sim 27$  min in Fig. 5a and  $\sim 30$  min in Fig. 5b. The nitrate adduct signal is already stabilized when that mode is engaged. In contrast to both the SIMPOL.1 predictions and the behavior observed for the *m*CPBA control, both synthesized OOM standards exhibit a distinctly different pattern: the peroxy acid and carboxylic acid signals rise simultaneously after sample introduction and follow nearly identical temporal profiles. This is reflected directly in the peroxy-to-carboxylic-acid ratio, which, after a brief stabilization period during the onset of evaporation, remains constant over time and reaches this steady level within only 1 to 2 min. Moreover, the signal intensities deviate strongly from expectations based on NMR measurements and SIMPOL-derived volatility differences: instead of the peroxy acids dominating and producing ratios higher than those measured by NMR, the carboxylic acid signals exceed the peroxy acid signals in most cases, with all measured ratios indicating a relative enrichment of carboxylic acids compared to the NMR values. Taken together, these observations support a consistent interpretation: the same parent species (predominantly the peroxy acids) evaporate into the gas phase, but a substantial fraction undergoes decomposition, yielding two detectable signals – one corresponding to the surviving peroxy acids and the other to the carboxylic acids formed upon decomposition.

Decomposition of peroxy acids could in principle occur during transport, ionization, or another step prior to detection. However, several lines of evidence indicate that structural degradation most likely occurs during ionization. The O–O bond in the peroxy acid group is relatively weak and susceptible to cleavage. In liquid-phase electrospray (H-ESI), high electric fields (Gabelica and Pauw, 2005) and electrochemical processes at the emitter (Pozniak and Cole, 2015) can promote such



170 bond rupture, particularly during (de)protonation pathways that impart considerable internal energy. Similarly, in gas-phase  
chemical ionization (MION2), proton-transfer reactions during collisions with reagent ions can destabilize the O–O bond,  
and electrostatic stress in the inlet may amplify this effect. By contrast, reagent ion adduct formation ionization (e.g., nitrate  
or uronium) is softer, relying on non-covalent clustering rather than covalent activation, and therefore better preserves fragile  
functionalities such as peroxy acid groups. This interpretation is consistent with the measured peroxy-to-carboxylic-acid ratios  
175 (Fig. 3), which show strong differences across ionization techniques (H-ESI vs. MION2), reagent ions (nitrate vs. uronium), and  
ionization mechanisms ((de)protonation vs. adduct formation), with higher ratios for adduct peaks compared to (de)protonated  
peaks. These systematic differences across ionization modes strongly support the conclusion that decomposition occurs during  
ionization, rather than elsewhere in the mass spectrometer; if fragmentation were occurring inside the instrument, the peroxy-  
to-carboxylic-acid ratios would not depend so sensitively on the ionization pathway. This interpretation is further reinforced  
180 by the operating conditions of the Orbitrap Exploris MX: during full-MS<sup>1</sup> acquisition, MS/MS fragmentation is not engaged,  
and ions are transmitted to the mass analyzer without deliberate collisional activation, making decomposition in the instrument  
unlikely. Furthermore, our observations align with earlier findings by Steimer et al. (2018), who reported rapid decay of  
synthesized monoperoxyipinic acid on filters – about 60 % lost within 5 h and measurable changes also in liquid samples over  
22 h, underscoring the intrinsic instability of peroxy acids related to atmospheric BVOC autoxidation.

185 Taken together, only the *m*CPBA control reflects the SIMPOL.1 volatility expectation that peroxy acids evaporate more  
readily than their corresponding carboxylic acids, leading to a significantly greater fraction of peroxy acids orbiting around  
the mass analyzer and, consequently, a much higher detected signal. This can plausibly be attributed to aromatic stabilization  
from the benzene ring, which renders *m*CPBA more persistent than typical aliphatic peroxy acids. In contrast, for all syn-  
thesized OOM standards, the systematically reduced peroxy-to-carboxylic-acid intensity ratios (relative to NMR) and their  
190 strong dependence on ionization chemistry are most consistent with ionization-induced decomposition of peroxy acids to the  
corresponding carboxylic acids.

Figure 6 compares intensities normalized to primary ions for nitrate and uronium adduct peaks of PNPA, PPA, and their  
corresponding carboxylic acids NPA and PA. The plotted values represent means with standard uncertainties from all mea-  
surements. Uronium adduct ionization consistently produced substantially higher intensities than nitrate adduct ionization,  
195 exceeding it by 1 to 2 orders of magnitude (factors ranging from  $4 \times 10^1$  to  $6 \times 10^2$ ). This trend is also reflected in the ab-  
solute intensities (see Fig. 5), indicating that the difference between the two ionization schemes is robust and not an artifact  
of normalization. Overall, these reagent-ion adduct intensity trends align well with chemical expectations. Nitrate is highly  
selective for HOMs and exhibits limited sensitivity to moderately oxygenated species (Riva et al., 2019b) such as PNPA, PPA,  
NPA, and PA. In contrast, uronium (protonated urea), a recently introduced positive-mode reagent, shows strong sensitivity for  
200 moderately oxygenated compounds (Shcherbinin et al., 2025), as evidenced by its consistently higher intensities than nitrate  
– also observable in blank measurements (Fig. 5) – confirming its suitability for this chemical space. On average, nitrate and  
uronium adduct signals for the peroxy acids were factors of 34 and 18 above their respective  $3\sigma$  blank thresholds, indicating  
that both channels operated well beyond their detection limits and that their behavior was unlikely to be governed by near-limit  
effects.

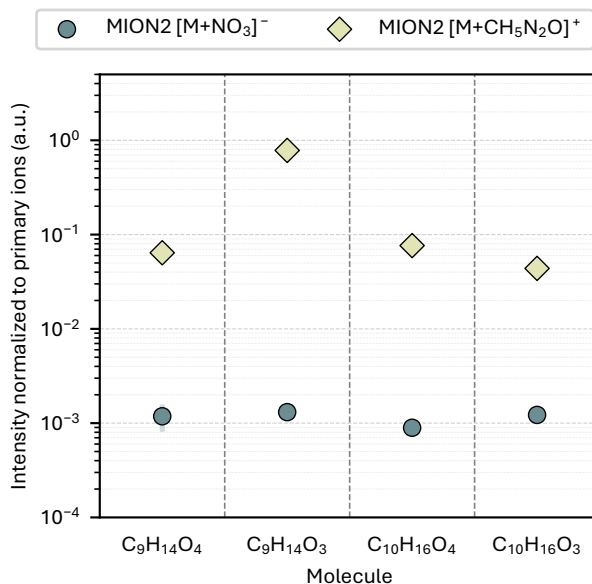


**Figure 6.** Intensities normalized to primary ions for nitrate and uronium adduct peaks of PNPA (C<sub>9</sub>H<sub>14</sub>O<sub>4</sub>), PPA (C<sub>10</sub>H<sub>16</sub>O<sub>4</sub>), and their corresponding carboxylic acids (NPA (C<sub>9</sub>H<sub>14</sub>O<sub>3</sub>) and PA (C<sub>10</sub>H<sub>16</sub>O<sub>3</sub>)). Symbols represent mean intensities, and shaded areas indicate standard uncertainties calculated from all repeated syntheses and measurements. If no error bar is visible, it is obscured by the symbol.

205 As seen in Fig. 3, the extent of peroxy acid loss depends on both the reagent-ion chemistry and the molecular structure of the analyte. Although uronium generally yields higher intensities than nitrate for both peroxy acids, it appears to induce greater in-source decomposition of PNPA while better preserving PPA; nonetheless, in both cases, the resulting peroxy-to-carboxylic-acid ratios remain substantially lower than expected from NMR and SIMPOL.1. This compound-specific behavior aligns with the uronium-CI mechanism: Shcherbinin et al. (2025) show that uronium ionization is fundamentally controlled by analyte-specific cluster geometries, binding enthalpies, and stabilization efficiencies, implying intrinsically molecule-dependent sensitivities. 210 Taken together, these observations add a final layer to our decomposition hypothesis: peroxy acid loss is dependent on both the ionization mechanism and the analyte.

#### 4 Conclusions

215 In this work, we synthesized monomeric OOM standards from  $\alpha$ -pinene ozonolysis as HOM proxies owing to their characteristic peroxy acid functionality. We characterized their detectability with a nitrate- and uronium-based MION-Orbitrap and compared these two gas-phase ionization schemes with liquid H-ESI.

Across all techniques, NMR confirmed that the freshly synthesized standards were dominated by peroxy acids, whereas Orbitrap measurements consistently yielded substantially lower peroxy-to-carboxylic-acid ratios, directly contradicting the SIMPOL.1 expectation that the higher volatility of peroxy acids should produce ratios even greater than those measured by NMR.



220 Crucially, the time evolution of these ratios hints at peroxy acid decomposition: after a brief stabilization period, the peroxy-to-  
carboxylic-acid ratios reach a constant level rapidly, and the peroxy and carboxylic acid signals exhibit near-identical temporal  
profiles. This behavior is inconsistent with volatility-driven separation but consistent with a single parent evaporating and then  
partially decomposing during ionization. The strong divergence between sample-preserving NMR and sample-modifying mass  
spectrometric measurements, together with the pronounced variability across ionization modes, indicates substantial in-source  
225 decomposition of peroxy acids during ionization, particularly under harder ionization pathways such as (de)protonation. Softer  
ionization routes such as nitrate and uronium adduct formation preserved the peroxy functionality more effectively, yet even  
these channels showed clear signatures of significant peroxy acid lability, reflecting a loss controlled by both reagent-ion chem-  
istry and the molecular structure of the analyte, as indicated by the pronounced shifts in the peroxy-to-carboxylic-acid ratios for  
the two standards under uronium ionization. Finally, our findings highlight that uronium adduct ionization captures this class  
230 of moderately oxygenated compounds far more efficiently than nitrate, underscoring its value as a complementary reagent for  
expanding molecular coverage beyond the HOM-biased selectivity of nitrate-CIMS.

Our results imply that peroxy acids formed via autoxidation of  $\alpha$ -pinene – and potentially other biogenic VOCs – may often  
be inaccurately quantified across commonly used mass spectrometric techniques. Because nitrate-CIMS is the most prevalent  
method for gas-phase HOM detection in new particle formation studies, such biases may translate into substantial uncertainties  
235 when deriving atmospheric process rates, including nucleation and growth rates of freshly formed particles. For example, in  
volatility-basis-set derivations from atmospheric measurements, misidentifying peroxy acids as carboxylic acids artificially  
lowers their assigned oxygen number, thereby underestimating O:C ratios for OOMs and propagating systematic errors in in-  
ferred volatilities. These findings underscore the need for calibration procedures that can capture such effects, together with  
continued exploration of novel reagent-ion chemistries that provide broader and more uniform coverage across the full range  
240 of molecular oxygenation states present in the atmosphere.

*Data availability.* The data are available from the authors upon request and will be made publicly available upon acceptance via a persistent  
identifier.

## Appendix A: Synthesis

### A1 General information

245 All reactions were stirred magnetically. Reagents were purchased from commercial suppliers and used as received. Dry  
dichloromethane (DCM) was retrieved from an Innovative Technologies PureSolv system.  $^1\text{H}$  and  $^{13}\text{C}$  NMR spectra were  
recorded on a Bruker AC 400 at 400 and 101 MHz; AC 600 at 600 and 151 MHz using the solvent peak as reference. The  
ratio of C9-peracid **4** and C9-acid **2** were determined by comparison of the signals at 2.77–2.67 ppm (m, 1H; for C9-peracid  
**4**) and 2.63–2.54 ppm (m, 1H; for C9-acid **2**). Multiplicities of  $^1\text{H}$  signals were referred to as s (singlet), d (doublet), t (triplet),  
250 q (quartet) and more complex patterns or m (multiplet).  $^{13}\text{C}$  NMR spectra were run in proton-decoupled mode. The ratio of

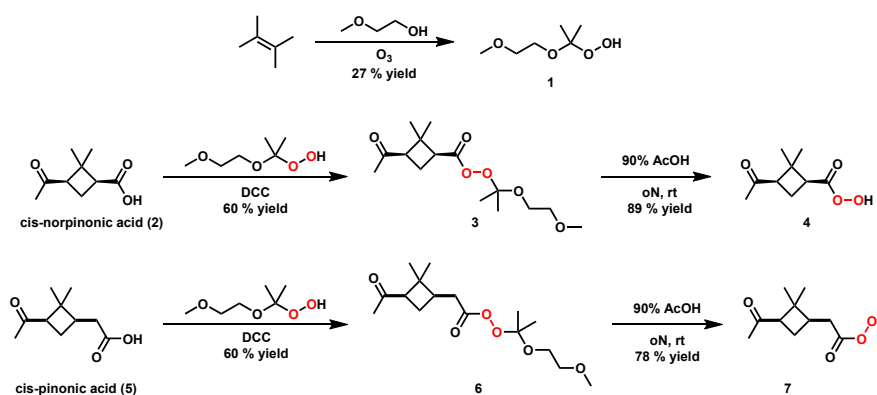


**Figure A1.** General scheme.

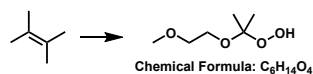


**Figure A2.** 2-Hydroperoxy-2-(2-methoxyethoxy)propane (1).

C10-peracid **7** and C10-acid **5** were determined by comparison of the signals at 31.28 ppm (for C10-peracid **7**) and 34.65 ppm (for C10-acid **5**). TLC-analysis was done with precoated aluminum-backed plates (Silica gel 60 F254, Merck). Compounds were visualized by submerging in: an acidic phosphomolybdic acid / Cerium sulphate solution,  $KMnO_4$ , Vanillin or Anisaldehyde and dried with a heat gun. Column chromatography was carried out with silica gel Merck 60. Eluent systems refer to volumetric ratios, e.g., 4:1 = 80% : 20%. Specific rotations were measured on an Anton Parr MCP 500 polarimeter at 20 °C and 589 nm.

## A2 General scheme

### A3 2-Hydroperoxy-2-(2-methoxyethoxy)propane (1)

A 100 mL Schlenk flask charged with 2,3-dimethylbut-2-ene (1.98 mL, 16.63 mmol, 1 equiv.) in 40 ml methoxyethanol. Subsequently, 10 drops Sudan III indicator (0.01 M in DCM) were added and the pink solution was cooled to -80 °C. After 5 minutes, a stream of  $O_3$  was passed through the reaction mixture until the pink color disappeared (approx. 8 minutes). Then, a stream of  $O_2$  was passed through for 5 minutes to remove excess  $O_3$ . The pale-yellow solution was directly subjected to distillation to remove the solvent. Subsequent high vacuum distillation furnished the desired product as colorless oil in 27 % yield (678 mg, 4.51 mmol).

b.p. 35 °C @ 0.75 mBar

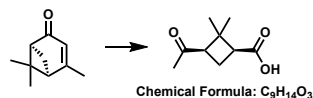


**Figure A3.** (1*S*,3*R*)-3-Acetyl-2,2-dimethylcyclobutane-1-carboxylic acid (*cis*-norpinonic acid (**2**)).

Analytical data in accordance with literature: Dussault et al. (1994).

#### A4 (1*S*,3*R*)-3-Acetyl-2,2-dimethylcyclobutane-1-carboxylic acid (*cis*-norpinonic acid (**2**))

A flame-dried 100 mL Schlenk flask was charged with (*S*)-Verbenone [CAS 1196-01-6] (95 %, 2.0 g, 12.6 mmol, 1 equiv.) and dissolved in 20 mL dry acetonitrile. The colorless solution was cooled to -40 °C and a stream of O<sub>3</sub> was passed through the reaction mixture until the reaction mixture became yellow (approx. 30 minutes). Then, a stream of O<sub>2</sub> was passed through for 5 minutes to remove excess O<sub>3</sub>. H<sub>2</sub>O<sub>2</sub> (35 % in water, 11.1 mL, 126 mmol, 10 equiv.) was added and the mixture was allowed to warm to room temperature. The aqueous layer was extracted with CHCl<sub>3</sub> (8x), dried over MgSO<sub>4</sub> and concentrated in vacuo. The desired product was obtained as white solids in 99 % yield (2.13 g, 12.5 mmol).

<sup>1</sup>H NMR (400 MHz, CDCl<sub>3</sub>) δ 2.90 (dd, *J* = 10.7, 7.7 Hz, 1H), 2.82 (ddd, *J* = 9.4, 7.9, 1.4 Hz, 1H), 2.61 (dtd, *J* = 12.8, 10.8, 2.0 Hz, 1H), 2.07 (d, *J* = 1.1 Hz, 3H), 1.90 (ddd, *J* = 11.8, 8.9, 6.7 Hz, 1H), 1.45 (d, *J* = 1.4 Hz, 3H), 0.97 (d, *J* = 1.7 Hz, 3H).

<sup>13</sup>C NMR (101 MHz, CDCl<sub>3</sub>) δ 207.3, 178.2, 53.1, 45.1, 45.0, 30.3, 30.1, 18.9, 18.1.

$[\alpha]_D^{20} = -52.58$  (c 1.60, CH<sub>2</sub>Cl<sub>2</sub>).

#### A5 2-(2-Methoxyethoxy)propan-2-yl (1*S*,3*R*)-3-acetyl-2,2-dimethylcyclobutane-1-carboperoxoat (**3**)

A 50 mL Schlenk flask was charged with *cis*-norpinonic acid (**2**) (1.27 g, 7.46 mmol, 1.2 equiv.) and *N,N*-dicyclohexylcarbodiimid (1.41 g, 6.84 mmol, 1.1 equiv.) in 30 mL dry DCM. To the white, turbid solution peroxide **1** (934 mg, 6.22 mmol, 1 equiv.) dissolved in 5 mL dry DCM was added, followed by 4-(dimethylamino)pyridine (76 mg, 0.62 mmol, 0.1 equiv.). The reaction was stirred at room temperature until TLC (petroleum ether/ethyl acetate 1:1, stained with anisaldehyde or vanillin stain) confirmed full conversion. Silica gel was added and all volatiles were removed in vacuo. The crude mixture was directly subjected to column chromatography (190 g silica, petroleum ether/ethyl acetate 2:1) and the desired product was obtained as colorless oil in 60 % yield (1.13 g, 3.73 mmol).

<sup>1</sup>H NMR (400 MHz, CDCl<sub>3</sub>) δ 3.77–3.69 (m, 2H), 3.51–3.43 (m, 2H), 3.34 (s, 3H), 2.94–2.85 (m, 1H), 2.85–2.75 (m, 1H), 2.75–2.61 (m, 1H), 2.05 (s, 3H), 1.99–1.87 (m, 1H), 1.47 (s, 6H), 1.42 (s, 3H), 0.98 (s, 3H).

<sup>13</sup>C NMR (101 MHz, CDCl<sub>3</sub>) δ 206.5, 169.0, 106.9, 71.9, 61.6, 59.2, 53.3, 45.1, 42.7, 30.4, 30.0, 23.4, 23.1, 19.2, 18.4.

$[\alpha]_D^{20} = -18.26$  (c 1.60, CH<sub>2</sub>Cl<sub>2</sub>).

HRMS (MION2-Orbitrap) [M + CH<sub>5</sub>N<sub>2</sub>O]<sup>+</sup> calculated 363.2131 u; found 363.2117 u.

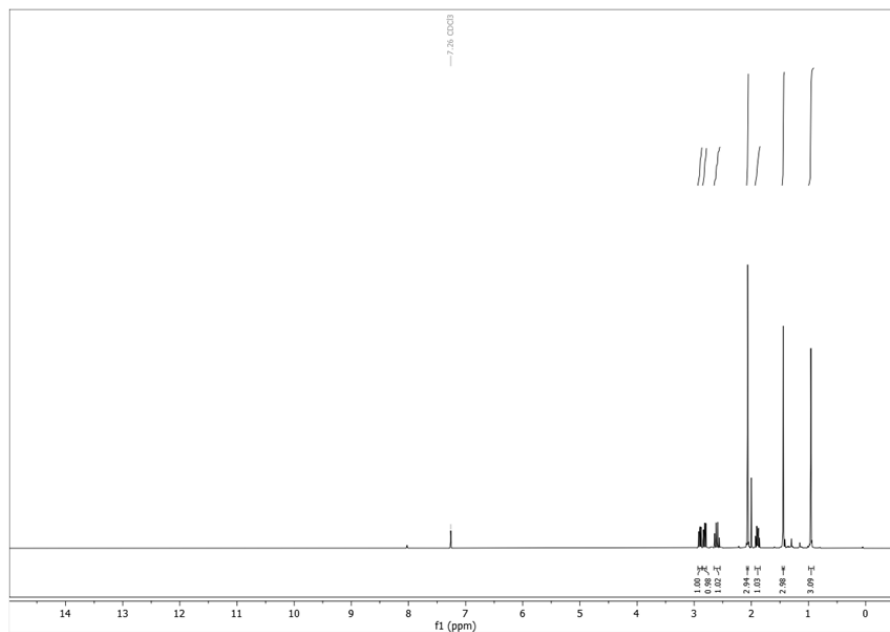


**Figure A4.** (1*S*,3*R*)-3-Acetyl-2,2-dimethylcyclobutane-1-carboxylic acid (*cis*-norpinonic acid (**2**)). <sup>1</sup>H NMR (400 MHz, CDCl<sub>3</sub>).

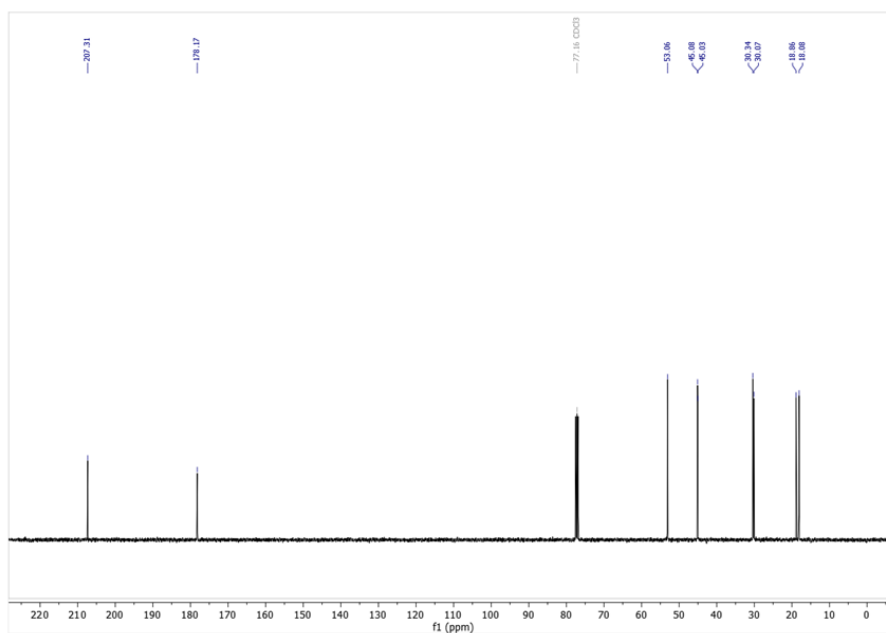


**Figure A5.** (1*S*,3*R*)-3-Acetyl-2,2-dimethylcyclobutane-1-carboxylic acid (*cis*-norpinonic acid (**2**)). <sup>13</sup>C NMR (101 MHz, CDCl<sub>3</sub>).



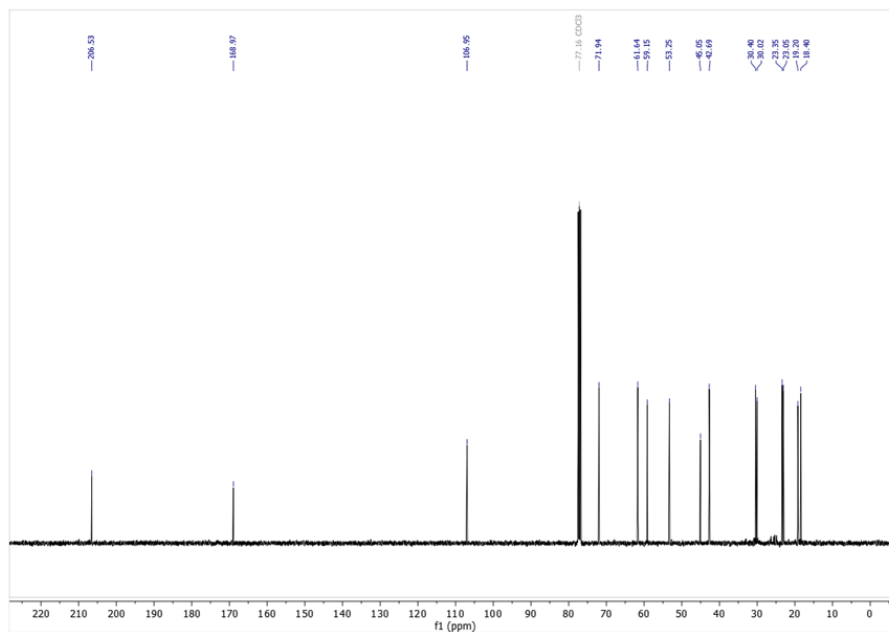


**Figure A8.** 2-(2-Methoxyethoxy)propan-2-yl (1*S*,3*R*)-3-acetyl-2,2-dimethylcyclobutane-1-carboperoxoate (**3**). <sup>13</sup>C NMR (101 MHz, CDCl<sub>3</sub>).

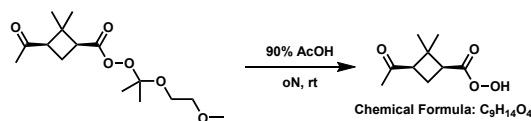


**Figure A9.** (1*S*,3*R*)-3-Acetyl-2,2-dimethylcyclobutane-1-carboperoxoic acid (**4**).

300 <sup>1</sup>H NMR (400 MHz, CDCl<sub>3</sub>)  $\delta$  11.33 (d,  $J$  = 3.4 Hz, 1H), 2.96 (dd,  $J$  = 10.6, 7.7 Hz, 1H), 2.90 (dd,  $J$  = 10.7, 8.0 Hz, 1H), 2.80–2.71 (m, 1H), 2.08 (s, 3H), 2.03–1.95 (m, 1H), 1.45 (s, 3H), 0.96 (s, 3H).

<sup>13</sup>C NMR (151 MHz, CDCl<sub>3</sub>)  $\delta$  206.5, 172.6, 53.2, 45.2, 42.1, 30.3, 30.0, 18.8, 18.3.

$[\alpha]_D^{20}$  = -11.24 (c 1.70, CH<sub>2</sub>Cl<sub>2</sub>).

#### A7 *Cis*-2-(2-Methoxyethoxy)propan-2-yl 2-(3-acetyl-2,2-dimethylcyclobutyl)ethaneperoxoate (**6**)

305 A 50 mL Schlenk flask was charged with commercially available *cis*-pinonic acid (**5**) [CAS 61826-55-9] (763 mg, 4.14 mmol, 1.2 equiv.) and *N,N*-dicyclohexylcarbodiimid (783 mg, 3.80 mmol, 1.1 equiv.) in 15 mL dry DCM. To the white, turbid solution peroxide **1** (518 mg, 3.45 mmol, 1 equiv.) dissolved in 2.5 mL dry DCM was added, followed by 4-(dimethylamino)pyridine (42 mg, 0.35 mmol, 0.1 equiv.). The reaction was stirred at room temperature until TLC (petroleum ether/ethyl acetate 1:1, stained with anisaldehyde or vanillin stain) confirmed full conversion. Silica gel was added and all volatiles were removed in

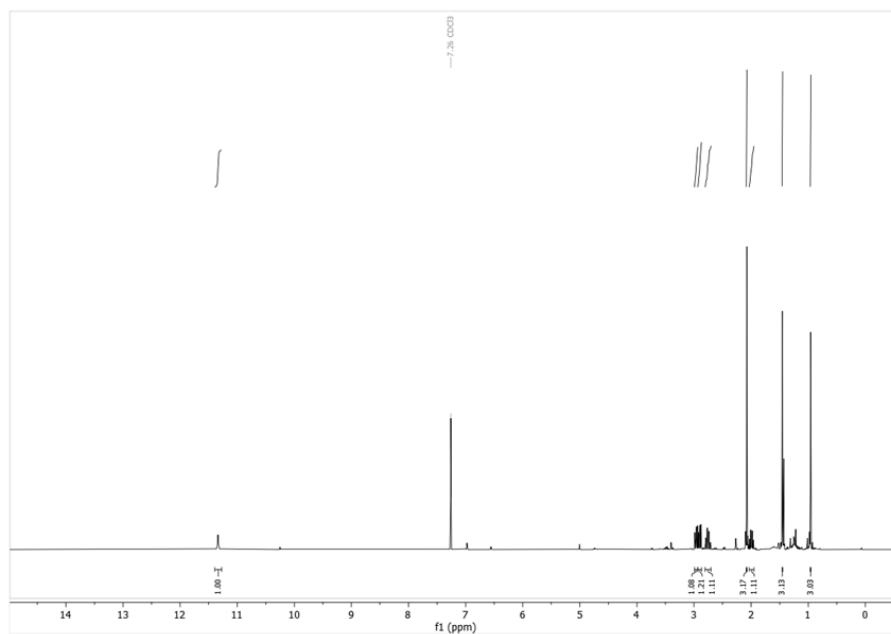


**Figure A10.** (1*S*,3*R*)-3-Acetyl-2,2-dimethylcyclobutane-1-carboxylic acid (**4**). <sup>1</sup>H NMR (400 MHz, CDCl<sub>3</sub>).

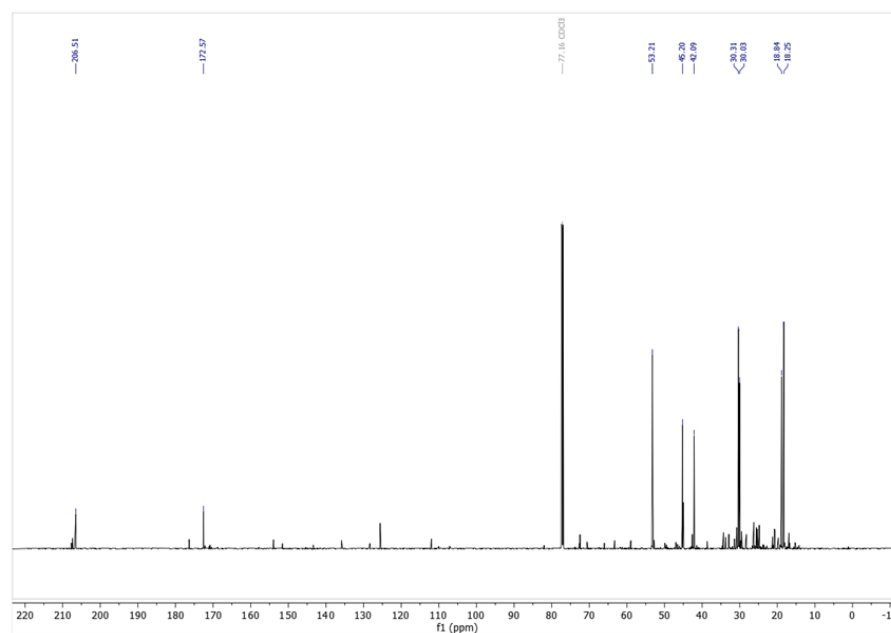


**Figure A11.** (1*S*,3*R*)-3-Acetyl-2,2-dimethylcyclobutane-1-carboxylic acid (**4**). <sup>13</sup>C NMR (151 MHz, CDCl<sub>3</sub>).

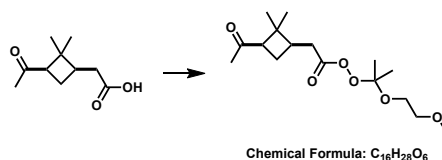


**Figure A12.** *Cis*-2-(2-Methoxyethoxy)propan-2-yl 2-(3-acetyl-2,2-dimethylcyclobutyl)ethaneperoxoate (**6**).

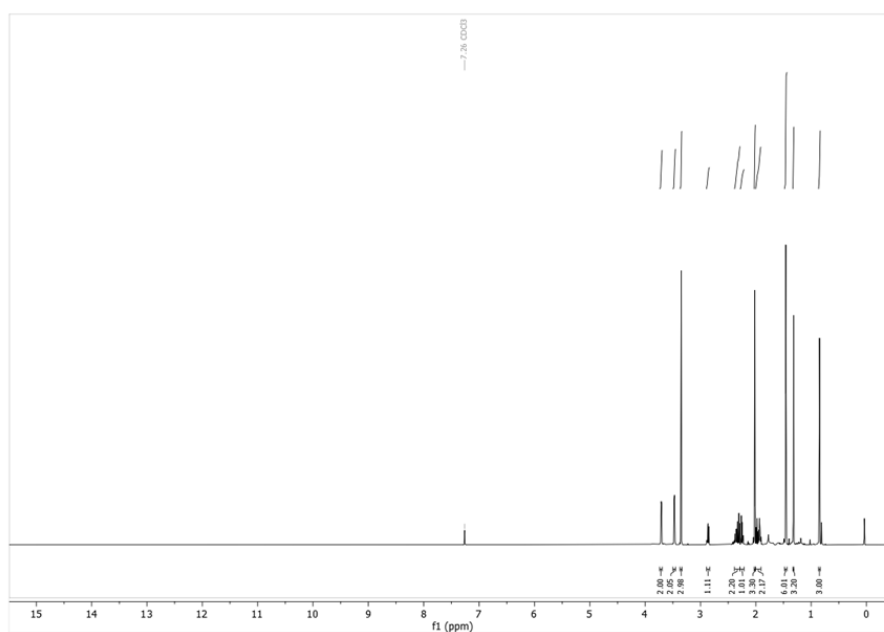


**Figure A13.** *Cis*-2-(2-Methoxyethoxy)propan-2-yl 2-(3-acetyl-2,2-dimethylcyclobutyl)ethaneperoxoate (**6**). <sup>1</sup>H NMR (600 MHz, CDCl<sub>3</sub>).

310 vacuo. The crude mixture was directly subjected to column chromatography (100 g silica, petroleum ether/ethyl acetate 2:1) and the desired product was obtained as white oily solids in 59 % yield (643 mg, 2.03 mmol).

<sup>1</sup>H NMR (600 MHz, CDCl<sub>3</sub>) δ 3.74–3.68 (m, 2H), 3.50–3.45 (m, 2H), 3.35 (s, 3H), 2.87 (dd, *J* = 10.2, 7.6 Hz, 1H), 2.40–2.29 (m, 2H), 2.24 (dd, *J* = 15.3, 7.6 Hz, 1H), 2.02 (s, 3H), 2.01–1.90 (m, 2H), 1.46 (s, 6H), 1.32 (s, 3H), 0.85 (s, 3H).

315 <sup>13</sup>C NMR (151 MHz, CDCl<sub>3</sub>) δ 207.3, 169.8, 107.0, 71.9, 61.6, 59.2, 54.2, 43.4, 38.0, 32.0, 30.3, 30.2, 23.1, 23.1, 23.1, 17.4.

HRMS (MION2-Orbitrap) [M + CH<sub>5</sub>N<sub>2</sub>O]<sup>+</sup> calculated 377.2288 u; found 377.2276 u.

#### **A8** *Cis*-2-(3-Acetyl-2,2-dimethylcyclobutyl)ethaneperoxoic acid (**7**)

A 100 mL round bottom flask charged with perester **6** (509 mg, 1.61 mmol, 1 equiv.) in 5.4 mL (freshly prepared) 90 % acetic acid (85.3 mmol, 53 equiv.) and BHT (0.1M solution in Et<sub>2</sub>O, 0.30 mL, 0.03 mmol, 0.02 equiv.). The clear colorless solution







## References

- 335 Alage, S., Michoud, V., Harb, S., Picquet-Varrault, B., Cirtog, M., Kumar, A., Rissanen, M., and Cantrell, C.: A nitrate ion chemical-ionization atmospheric-pressure-interface time-of-flight mass spectrometer ( $\text{NO}_3^-$  ToFCIMS) sensitivity study, *Atmospheric Measurement Techniques*, 17, 4709–4724, <https://doi.org/10.5194/amt-17-4709-2024>, 2024.
- Bianchi, F., Kurtén, T., Riva, M., Mohr, C., Rissanen, M. P., Roldin, P., Berndt, T., Crouse, J. D., Wennberg, P. O., Mentel, T. F., Wildt, J., Junninen, H., Jokinen, T., Kulmala, M., Worsnop, D. R., Thornton, J. A., Donahue, N., Kjaergaard, H. G., and Ehn, M.: Highly Oxygenated Organic Molecules (HOM) from Gas-Phase Autoxidation Involving Peroxy Radicals: A Key Contributor to Atmospheric Aerosol, *Chemical Reviews*, 119, 3472–3509, <https://doi.org/10.1021/acs.chemrev.8b00395>, 2019.
- 340 Cai, C., Zhang, X., Wang, K., Zhang, Y., Wang, L., Zhang, Q., Duan, F., He, K., and Yu, S.-C.: Incorporation of new particle formation and early growth treatments into WRF/Chem: Model improvement, evaluation, and impacts of anthropogenic aerosols over East Asia, *Atmospheric Environment*, 124, 262–284, <https://doi.org/10.1016/j.atmosenv.2015.05.046>, 2016.
- 345 Cai, R., Mikkilä, J., Bengs, A., Koirala, M., Mikkilä, J., Holm, S., Juuti, P., Meder, M., Partovi, F., Shcherbinin, A., Worsnop, D., Ehn, M., and Kangasluoma, J.: Extending the Range of Detectable Trace Species with the Fast Polarity Switching of Chemical Ionization Orbitrap Mass Spectrometry, *Analytical Chemistry*, 96, 8604–8612, <https://doi.org/10.1021/acs.analchem.4c00650>, 2024.
- Donahue, N. M., Robinson, A. L., and Pandis, S. N.: Atmospheric organic particulate matter: From smoke to secondary organic aerosol, *Atmospheric Environment*, 43, 94–106, <https://doi.org/10.1016/j.atmosenv.2008.09.055>, 2009.
- 350 Dussault, P. H., Zope, U. R., and Westermeyer, T. A.: 2-(2-Methoxyethoxy)prop-2-yl Hydroperoxide: An Easily Handled Reagent for the Synthesis of Alkyl Hydroperoxides, *The Journal of Organic Chemistry*, 59, 8267–8268, <https://doi.org/10.1021/jo00105a053>, 1994.
- Ehn, M., Thornton, J. A., Kleist, E., Sipilä, M., Junninen, H., Pullinen, I., Springer, M., Rubach, F., Tillmann, R., Lee, B., Lopez-Hilfiker, F., Andres, S., Acir, I.-H., Rissanen, M., Jokinen, T., Schobesberger, S., Kangasluoma, J., Kontkanen, J., Nieminen, T., Kurtén, T., Nielsen, L. B., Jørgensen, S., Kjaergaard, H. G., Canagaratna, M., Maso, M. D., Berndt, T., Petäjä, T., Wahner, A., Kerminen, V.-M., Kulmala, M., Worsnop, D. R., Wildt, J., and Mentel, T. F.: A large source of low-volatility secondary organic aerosol, *Nature*, 506, 476–479, <https://doi.org/10.1038/nature13032>, 2014.
- 355 Elm, J., Myllys, N., and Kurtén, T.: What Is Required for Highly Oxidized Molecules To Form Clusters with Sulfuric Acid?, *The Journal of Physical Chemistry A*, 121, 4578–4587, <https://doi.org/10.1021/acs.jpca.7b03759>, 2017.
- Fountoukis, C., Riipinen, I., Denier van der Gon, H. a. C., Charalampidis, P. E., Pilinis, C., Wiedensohler, A., O’Dowd, C., Putaud, J. P., Moerman, M., and Pandis, S. N.: Simulating ultrafine particle formation in Europe using a regional CTM: contribution of primary emissions versus secondary formation to aerosol number concentrations, *Atmospheric Chemistry and Physics*, 12, 8663–8677, <https://doi.org/10.5194/acp-12-8663-2012>, 2012.
- 360 Gabelica, V. and Pauw, E. D.: Internal energy and fragmentation of ions produced in electrospray sources, *Mass Spectrometry Reviews*, 24, 566–587, <https://doi.org/10.1002/mas.20027>, 2005.
- Gordon, H., Kirkby, J., Baltensperger, U., Bianchi, F., Breitenlechner, M., Curtius, J., Dias, A., Dommen, J., Donahue, N. M., Dunne, E. M., Duplissy, J., Ehrhart, S., Flagan, R. C., Frege, C., Fuchs, C., Hansel, A., Hoyle, C. R., Kulmala, M., Kürten, A., Lehtipalo, K., Makhmutov, V., Molteni, U., Rissanen, M. P., Stozkhov, Y., Tröstl, J., Tsagkogeorgas, G., Wagner, R., Williamson, C., Wimmer, D., Winkler, P. M., Yan, C., and Carslaw, K. S.: Causes and importance of new particle formation in the present-day and preindustrial atmospheres, *Journal of Geophysical Research: Atmospheres*, 122, 8739–8760, <https://doi.org/10.1002/2017JD026844>, 2017.



- 370 Hallquist, M., Wenger, J. C., Baltensperger, U., Rudich, Y., Simpson, D., Claeys, M., Dommen, J., Donahue, N. M., George, C., Goldstein, A. H., Hamilton, J. F., Herrmann, H., Hoffmann, T., Iinuma, Y., Jang, M., Jenkin, M. E., Jimenez, J. L., Kiendler-Scharr, A., Maenhaut, W., McFiggans, G., Mentel, T. F., Monod, A., Prévôt, A. S. H., Seinfeld, J. H., Surratt, J. D., Szmigielski, R., and Wildt, J.: The formation, properties and impact of secondary organic aerosol: current and emerging issues, *Atmospheric Chemistry and Physics*, 9, 5155–5236, <https://doi.org/10.5194/acp-9-5155-2009>, 2009.
- 375 Hatakeyama, S., Izumi, K., Fukuyama, T., and Akimoto, H.: Reactions of ozone with  $\alpha$ -pinene and  $\beta$ -pinene in air: Yields of gaseous and particulate products, *Journal of Geophysical Research: Atmospheres*, 94, 13 013–13 024, <https://doi.org/10.1029/JD094iD10p13013>, 1989.
- HEI: State of Global Air Report 2025, Health Effects Institute (HEI), Boston, MA, <https://www.stateofglobalair.org/resources/report/state-global-air-report-2025>, 2025.
- 380 Hodzic, A., Kasibhatla, P. S., Jo, D. S., Cappa, C. D., Jimenez, J. L., Madronich, S., and Park, R. J.: Rethinking the global secondary organic aerosol (SOA) budget: stronger production, faster removal, shorter lifetime, *Atmospheric Chemistry and Physics*, 16, 7917–7941, <https://doi.org/10.5194/acp-16-7917-2016>, 2016.
- IHME: Global Burden of Disease 2023: Findings from the GBD 2023 study, Institute for Health Metrics and Evaluation (IHME), Seattle, WA, <https://www.healthdata.org/research-analysis/library/global-burden-disease-2023-findings-gbd-2023-study>, 2025.
- 385 IPCC: Climate Change 2021: The Physical Science Basis, Contribution of Working Group I to the Sixth Assessment Report of the Intergovernmental Panel on Climate Change [Masson-Delmotte, V., P. Zhai, A. Pirani, S.L. Connors, C. Péan, S. Berger, N. Caud, Y. Chen, L. Goldfarb, M.I. Gomis, M. Huang, K. Leitzell, E. Lonnoy, J.B.R. Matthews, T.K. Maycock, T. Waterfield, O. Yelekçi, R. Yu, and B. Zhou (eds.)], Cambridge University Press, Cambridge, United Kingdom and New York, NY, USA, 2391 pp, <https://doi.org/10.1017/9781009157896>, 2021.
- 390 Jimenez, J. L., Canagaratna, M. R., Donahue, N. M., Prevot, A. S. H., Zhang, Q., Kroll, J. H., DeCarlo, P. F., Allan, J. D., Coe, H., Ng, N. L., Aiken, A. C., Docherty, K. S., Ulbrich, I. M., Grieshop, A. P., Robinson, A. L., Duplissy, J., Smith, J. D., Wilson, K. R., Lanz, V. A., Hueglin, C., Sun, Y. L., Tian, J., Laaksonen, A., Raatikainen, T., Rautiainen, J., Vaattovaara, P., Ehn, M., Kulmala, M., Tomlinson, J. M., Collins, D. R., Cubison, M. J., E., Dunlea, J., Huffman, J. A., Onasch, T. B., Alfarra, M. R., Williams, P. I., Bower, K., Kondo, Y., Schneider, J., Drewnick, F., Borrmann, S., Weimer, S., Demerjian, K., Salcedo, D., Cottrell, L., Griffin, R., Takami, A., Miyoshi, T.,  
395 Hatakeyama, S., Shimono, A., Sun, J. Y., Zhang, Y. M., Dzepina, K., Kimmel, J. R., Sueper, D., Jayne, J. T., Herndon, S. C., Trimborn, A. M., Williams, L. R., Wood, E. C., Middlebrook, A. M., Kolb, C. E., Baltensperger, U., and Worsnop, D. R.: Evolution of Organic Aerosols in the Atmosphere, *Science*, 326, 1525–1529, <https://doi.org/10.1126/science.1180353>, 2009.
- Kavouras, I. G., Mihalopoulos, N., and Stephanou, E. G.: Formation and gas/particle partitioning of monoterpenes photo-oxidation products over forests, *Geophysical Research Letters*, 26, 55–58, <https://doi.org/10.1029/1998GL900251>, 1999.
- 400 Kenseth, C. M., Hafeman, N. J., Huang, Y., Dalleska, N. F., Stoltz, B. M., and Seinfeld, J. H.: Synthesis of Carboxylic Acid and Dimer Ester Surrogates to Constrain the Abundance and Distribution of Molecular Products in  $\alpha$ -Pinene and  $\beta$ -Pinene Secondary Organic Aerosol, *Environmental Science & Technology*, 54, 12 829–12 839, <https://doi.org/10.1021/acs.est.0c01566>, 2020.
- Kenseth, C. M., Hafeman, N. J., Rezgui, S. P., Chen, J., Huang, Y., Dalleska, N. F., Kjaergaard, H. G., Stoltz, B. M., Seinfeld, J. H., and Wennberg, P. O.: Particle-phase accretion forms dimer esters in pinene secondary organic aerosol, *Science*, 382, 787–792, <https://doi.org/10.1126/science.adi0857>, 2023.
- 405 Kirkby, J., Duplissy, J., Sengupta, K., Frege, C., Gordon, H., Williamson, C., Heinritzi, M., Simon, M., Yan, C., Almeida, J., Tröstl, J., Nieminen, T., Ortega, I. K., Wagner, R., Adamov, A., Amorim, A., Bernhammer, A.-K., Bianchi, F., Breitenlechner, M., Brilke, S., Chen,



- X., Craven, J., Dias, A., Ehrhart, S., Flagan, R. C., Franchin, A., Fuchs, C., Guida, R., Hakala, J., Hoyle, C. R., Jokinen, T., Junninen, H., Kangasluoma, J., Kim, J., Krapf, M., Kürten, A., Laaksonen, A., Lehtipalo, K., Makhmutov, V., Mathot, S., Molteni, U., Onnela, A.,  
410 Peräkylä, O., Piel, F., Petäjä, T., Praplan, A. P., Pringle, K., Rap, A., Richards, N. A. D., Riipinen, I., Rissanen, M. P., Rondo, L., Sarnela, N., Schobesberger, S., Scott, C. E., Seinfeld, J. H., Sipilä, M., Steiner, G., Stozhkov, Y., Stratmann, F., Tomé, A., Virtanen, A., Vogel, A. L., Wagner, A. C., Wagner, P. E., Weingartner, E., Wimmer, D., Winkler, P. M., Ye, P., Zhang, X., Hansel, A., Dommen, J., Donahue, N. M., Worsnop, D. R., Baltensperger, U., Kulmala, M., Carslaw, K. S., and Curtius, J.: Ion-induced nucleation of pure biogenic particles, *Nature*, 533, 521–526, <https://doi.org/10.1038/nature17953>, 2016.
- 415 Kulmala, M.: How Particles Nucleate and Grow, *Science*, 302, 1000–1001, <https://doi.org/10.1126/science.1090848>, 2003.
- Kurtén, T., Rissanen, M. P., Mackeprang, K., Thornton, J. A., Hyttinen, N., Jørgensen, S., Ehn, M., and Kjaergaard, H. G.: Computational Study of Hydrogen Shifts and Ring-Opening Mechanisms in  $\alpha$ -Pinene Ozonolysis Products, *The Journal of Physical Chemistry A*, 119, 11 366–11 375, <https://doi.org/10.1021/acs.jpca.5b08948>, 2015.
- Li, K., Resch, J., and Kalberer, M.: Synthesis and Characterization of Organic Peroxides from Monoterpene-Derived Criegee Intermediates  
420 in Secondary Organic Aerosol, *Environmental Science & Technology*, 58, 3322–3331, <https://doi.org/10.1021/acs.est.3c07048>, 2024.
- Lupascu, A., Easter, R., Zaveri, R., Shrivastava, M., Pekour, M., Tomlinson, J., Yang, Q., Matsui, H., Hodzic, A., Zhang, Q., and Fast, J. D.: Modeling particle nucleation and growth over northern California during the 2010 CARES campaign, *Atmospheric Chemistry and Physics*, 15, 12 283–12 313, <https://doi.org/10.5194/acp-15-12283-2015>, 2015.
- Matsui, H., Koike, M., Takegawa, N., Kondo, Y., Takami, A., Takamura, T., Yoon, S., Kim, S.-W., Lim, H.-C., and Fast, J. D.: Spatial and  
425 temporal variations of new particle formation in East Asia using an NPF-explicit WRF-chem model: North-south contrast in new particle formation frequency, *Journal of Geophysical Research: Atmospheres*, 118, 11,647–11,663, <https://doi.org/10.1002/jgrd.50821>, 2013.
- Mettke, P., Mutzel, A., Böge, O., Herrmann, H., Mettke, P., Mutzel, A., Böge, O., and Herrmann, H.: Synthesis and Characterization of Atmospherically Relevant Hydroxy Hydroperoxides, *Atmosphere*, 13, <https://doi.org/10.3390/atmos13040507>, 2022.
- Pankow, J. F. and Asher, W. E.: SIMPOL.1: a simple group contribution method for predicting vapor pressures and enthalpies of vaporization  
430 of multifunctional organic compounds, *Atmospheric Chemistry and Physics*, 8, 2773–2796, <https://doi.org/10.5194/acp-8-2773-2008>, 2008.
- Posner, L. N. and Pandis, S. N.: Sources of ultrafine particles in the Eastern United States, *Atmospheric Environment*, 111, 103–112, <https://doi.org/10.1016/j.atmosenv.2015.03.033>, 2015.
- Pozniak, B. P. and Cole, R. B.: Perspective on Electrospray Ionization and Its Relation to Electrochemistry, *Journal of the American Society for Mass Spectrometry*, 26, 369–385, <https://doi.org/10.1007/s13361-014-1066-x>, 2015.
- 435 Qi, X., Ding, A., Roldin, P., Xu, Z., Zhou, P., Sarnela, N., Nie, W., Huang, X., Rusanen, A., Ehn, M., Rissanen, M. P., Petäjä, T., Kulmala, M., and Boy, M.: Modelling studies of HOMs and their contributions to new particle formation and growth: comparison of boreal forest in Finland and a polluted environment in China, *Atmospheric Chemistry and Physics*, 18, 11 779–11 791, <https://doi.org/10.5194/acp-18-11779-2018>, 2018.
- 440 Reddington, C. L., Carslaw, K. S., Spracklen, D. V., Frontoso, M. G., Collins, L., Merikanto, J., Minikin, A., Hamburger, T., Coe, H., Kulmala, M., Aalto, P., Flentje, H., Plass-Dülmer, C., Birmili, W., Wiedensohler, A., Wehner, B., Tuch, T., Sonntag, A., O’Dowd, C. D., Jennings, S. G., Dupuy, R., Baltensperger, U., Weingartner, E., Hansson, H.-C., Tunved, P., Laj, P., Sellegri, K., Boulon, J., Putaud, J.-P., Gruening, C., Swietlicki, E., Roldin, P., Henzing, J. S., Moerman, M., Mihalopoulos, N., Kouvarakis, G., Ždímal, V., Zíková, N., Marinoni, A., Bonasoni, P., and Duchi, R.: Primary versus secondary contributions to particle number concentrations in the European boundary layer,  
445 *Atmospheric Chemistry and Physics*, 11, 12 007–12 036, <https://doi.org/10.5194/acp-11-12007-2011>, 2011.



- Rissanen, M. P., Mikkilä, J., Iyer, S., and Hakala, J.: Multi-scheme chemical ionization inlet (MION) for fast switching of reagent ion chemistry in atmospheric pressure chemical ionization mass spectrometry (CIMS) applications, *Atmospheric Measurement Techniques*, 12, 6635–6646, <https://doi.org/10.5194/amt-12-6635-2019>, 2019.
- Riva, M., Ehn, M., Li, D., Tomaz, S., Bourgain, F., Perrier, S., and George, C.: CI-Orbitrap: An Analytical Instrument To Study Atmospheric Reactive Organic Species, *Analytical Chemistry*, 91, 9419–9423, <https://doi.org/10.1021/acs.analchem.9b02093>, 2019a.
- Riva, M., Rantala, P., Krechmer, J. E., Peräkylä, O., Zhang, Y., Heikkinen, L., Garmash, O., Yan, C., Kulmala, M., Worsnop, D., and Ehn, M.: Evaluating the performance of five different chemical ionization techniques for detecting gaseous oxygenated organic species, *Atmospheric Measurement Techniques*, 12, 2403–2421, <https://doi.org/10.5194/amt-12-2403-2019>, 2019b.
- Shcherbinin, A., Finkenzeller, H., Mikkilä, J., Kontro, J., Vinkvist, N., Kangasluoma, J., and Rissanen, M.: From Hydrocarbons to Highly Functionalized Molecules in a Single Measurement: Comprehensive Analysis of Complex Gas Mixtures by Multi-Pressure Chemical Ionization Mass Spectrometry, *Analytical Chemistry*, 96, 19926–19932, <https://doi.org/10.1021/acs.analchem.4c03859>, 2024.
- Shcherbinin, A., Finkenzeller, H., Partovi, F., Vinkvist, N., Kontro, J., Boyer, M., Mikkilä, J., Iyer, S., Mikkilä, J., Juuti, P., Sarnela, N., Kangasluoma, J., and Rissanen, M.: Uronium from X-ray-Desorbed Urea Enables Sustainable Ultrasensitive Detection of Amines and Semivolatiles, *Analytical Chemistry*, 97, 21282–21290, <https://doi.org/10.1021/acs.analchem.5c02239>, 2025.
- Sindelarova, K., Markova, J., Simpson, D., Huszar, P., Karlicky, J., Darras, S., and Granier, C.: High-resolution biogenic global emission inventory for the time period 2000–2019 for air quality modelling, *Earth System Science Data*, 14, 251–270, <https://doi.org/10.5194/essd-14-251-2022>, 2022.
- Steimer, S. S., Delvaux, A., Campbell, S. J., Gallimore, P. J., Grice, P., Howe, D. J., Pitton, D., Claeys, M., Hoffmann, T., and Kalberer, M.: Synthesis and characterisation of peroxy-pinic acids as proxies for highly oxygenated molecules (HOMs) in secondary organic aerosol, *Atmospheric Chemistry and Physics*, 18, 10973–10983, <https://doi.org/10.5194/acp-18-10973-2018>, 2018.
- Stolzenburg, D., Fischer, L., Vogel, A. L., Heinritzi, M., Schervish, M., Simon, M., Wagner, A. C., Dada, L., Ahonen, L. R., Amorim, A., Baccarini, A., Bauer, P. S., Baumgartner, B., Bergen, A., Bianchi, F., Breitenlechner, M., Brilke, S., Buenrostro Mazon, S., Chen, D., Dias, A., Draper, D. C., Duplissy, J., El Haddad, I., Finkenzeller, H., Frege, C., Fuchs, C., Garmash, O., Gordon, H., He, X., Helm, J., Hofbauer, V., Hoyle, C. R., Kim, C., Kirkby, J., Kontkanen, J., Kürten, A., Lampilahti, J., Lawler, M., Lehtipalo, K., Leiminger, M., Mai, H., Mathot, S., Mentler, B., Molteni, U., Nie, W., Nieminen, T., Nowak, J. B., Ojdanic, A., Onnela, A., Passananti, M., Petäjä, T., Quéléver, L. L. J., Rissanen, M. P., Sarnela, N., Schallhart, S., Tauber, C., Tomé, A., Wagner, R., Wang, M., Weitz, L., Wimmer, D., Xiao, M., Yan, C., Ye, P., Zha, Q., Baltensperger, U., Curtius, J., Dommen, J., Flagan, R. C., Kulmala, M., Smith, J. N., Worsnop, D. R., Hansel, A., Donahue, N. M., and Winkler, P. M.: Rapid growth of organic aerosol nanoparticles over a wide tropospheric temperature range, *Proceedings of the National Academy of Sciences*, 115, 9122–9127, <https://doi.org/10.1073/pnas.1807604115>, 2018.
- Stolzenburg, D., Wang, M., Schervish, M., and Donahue, N. M.: Tutorial: Dynamic organic growth modeling with a volatility basis set, *Journal of Aerosol Science*, 166, 106063, <https://doi.org/10.1016/j.jaerosci.2022.106063>, 2022.
- Tröstl, J., Chuang, W. K., Gordon, H., Heinritzi, M., Yan, C., Molteni, U., Ahlm, L., Frege, C., Bianchi, F., Wagner, R., Simon, M., Lehtipalo, K., Williamson, C., Craven, J. S., Duplissy, J., Adamov, A., Almeida, J., Bernhammer, A.-K., Breitenlechner, M., Brilke, S., Dias, A., Ehrhart, S., Flagan, R. C., Franchin, A., Fuchs, C., Guida, R., Gysel, M., Hansel, A., Hoyle, C. R., Jokinen, T., Junninen, H., Kangasluoma, J., Keskinen, H., Kim, J., Krapf, M., Kürten, A., Laaksonen, A., Lawler, M., Leiminger, M., Mathot, S., Möhler, O., Nieminen, T., Onnela, A., Petäjä, T., Piel, F. M., Miettinen, P., Rissanen, M. P., Rondo, L., Sarnela, N., Schobesberger, S., Sengupta, K., Sipilä, M., Smith, J. N., Steiner, G., Tomé, A., Virtanen, A., Wagner, A. C., Weingartner, E., Wimmer, D., Winkler, P. M., Ye, P., Carslaw, K. S., Curtius,



- J., Dommen, J., Kirkby, J., Kulmala, M., Riipinen, I., Worsnop, D. R., Donahue, N. M., and Baltensperger, U.: The role of low-volatility organic compounds in initial particle growth in the atmosphere, *Nature*, 533, 527–531, <https://doi.org/10.1038/nature18271>, 2016.
- 485 Wilson, W. E., Schwartz, W. E., and Kinzer, G. W.: Haze formation: Its nature and origin, Tech. Rep. prepared for the Environmental Protection Agency (CPA 70-Neg. 172) and Coordinating Research Council (CAPA 6-68), Battelle Columbus Laboratories, 1972.
- Yu, F. and Luo, G.: Simulation of particle size distribution with a global aerosol model: contribution of nucleation to aerosol and CCN number concentrations, *Atmospheric Chemistry and Physics*, 9, 7691–7710, <https://doi.org/10.5194/acp-9-7691-2009>, 2009.
- 490 Yu, J., Griffin, R. J., Cocker III, D. R., Flagan, R. C., Seinfeld, J. H., and Blanchard, P.: Observation of gaseous and particulate products of monoterpene oxidation in forest atmospheres, *Geophysical Research Letters*, 26, 1145–1148, <https://doi.org/10.1029/1999GL900169>, 1999.
- Zhang, Q., Jimenez, J. L., Canagaratna, M. R., Allan, J. D., Coe, H., Ulbrich, I., Alfarra, M. R., Takami, A., Middlebrook, A. M., Sun, Y. L., Dzepina, K., Dunlea, E., Docherty, K., DeCarlo, P. F., Salcedo, D., Onasch, T., Jayne, J. T., Miyoshi, T., Shimo, A., Hatakeyama, S., Takegawa, N., Kondo, Y., Schneider, J., Drewnick, F., Borrmann, S., Weimer, S., Demerjian, K., Williams, P., Bower, K., Bahreini, R., Cottrell, L., Griffin, R. J., Rautiainen, J., Sun, J. Y., Zhang, Y. M., and Worsnop, D. R.: Ubiquity and dominance of oxygenated species in organic aerosols in anthropogenically-influenced Northern Hemisphere midlatitudes, *Geophysical Research Letters*, 34, <https://doi.org/10.1029/2007GL029979>, 2007.